AD-A117 313 ARMY ARMAMENT RESEARCH AND DEVELOPMENT COMMAND ABERD--ETC F/G 19/1
COMPUTATIONS OF PROJECTILE MAGNUS EFFECT AT TRANSONIC VELOCITIE--ETC(U)
JUN 82 C J NIETUBICZ, W B STUREK, K R HEAVEY

UNCLASSIFIED NL

END
DATE FILMED
8-82
DTIC

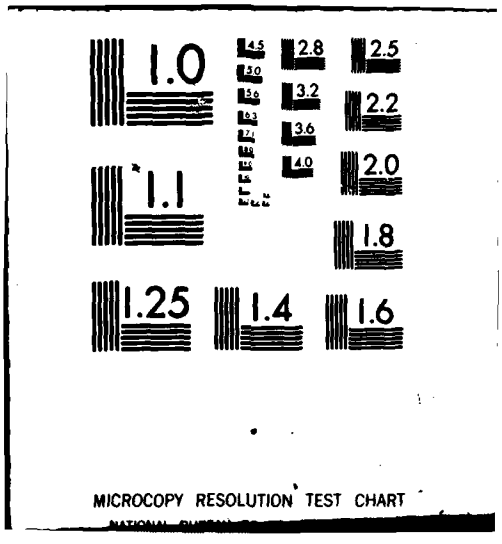
1.0
1.1
1.25
1.4
1.6
1.8
2.0
2.2
2.5
2.8
3.2
3.6
4.0
4.5
5.0
5.6
MICROCOPY RESOLUTION TEST CHART

18 JUN 1982

COMPUTATIONS OF PROJECTILE MAGNUS EFFECT AT TRANSONIC VELOCITIES

CHARLES J. NIETUBICZ*, Mr., WALTER B. STUREK, Dr.,
and KAREN R. HEAVEY, Mrs.
U.S. Army Ballistic Research Laboratory/ARRADCOM
Aberdeen Proving Ground, Maryland 21005

I. INTRODUCTION

The accurate prediction or experimental determination of projectile aerodynamics is of significant importance to the shell designer and ballistician. The shell designer requires accurate aerodynamic data for the overall development of new shell. The ballistician is concerned with the development of aiming data and therefore relies heavily on accurate aerodynamic data. Experimental costs have sky rocketed in recent years and have contributed significantly to overall system development costs. Computational techniques are beginning to show promise as a means to alleviate or at least temper these rising development costs by providing relatively low cost computer analysis of new designs. As computer technology increases and machines become faster with larger memory, the use of computational methods in design becomes more of a reality.

The means to compute projectile aerodynamics for all Mach number regimes covered by a given projectile in its flight history has been an area of research actively pursued by the Aerodynamics Research Branch of the Ballistic Research Laboratory. Early work had focused on the supersonic flight regime and, in particular on the accurate prediction of the Magnus force. The Magnus force, which is very small in magnitude (on the order of 1/10 the normal force), is a critical parameter in determining the dynamic stability of shell. The Magnus force is generated by a spin induced distortion of the boundary layer; therefore, correct modeling of the viscous/inviscid interation is critical for accurate computations. The work of Sturek, et. al.[1] has shown that accurate results in the supersonic regime can be obtained for ogive-cylinder projectile shapes. This technique involved separate computations of the turbulent, viscous boundary layer and the outer inviscid flow field. As the projectile shapes were generalized to include boattails, more sophisticated computational techniques had to be employed. These new methods, which solved the thin-layer Navier Stokes equations, were successfully applied to ogive-cylinder-boattail shapes by Sturek and Schiff[2,3]. The solution of the Navier Stokes

equations allows for the simultaneous computation of the viscous/inviscid flow field and thus provided the basis for good Magnus force prediction.

A region of critical aerodynamic behavior occurs in the high transonic regime, $0.90 < M < 1.15$, where aerodynamic coefficients have been found to increase by as much as 100%. This flight velocity regime is both experimentally and computationally difficult. Thus, only a small amount of experimental data are available for design studies and only limited computational studies have been made. An initial attempt to develop a computational capability suitable for Magnus prediction at transonic velocity was made by Nietubicz, et. al[4] whereby the thin-layer Navier Stokes computational technique was applied to standard and hollow projectile shapes at zero degrees angle of attack. Computational results were also obtained for non-spinning projectiles at angle of attack[5]; however limitations of computer resources (CDC 7600) became apparent. In this paper, recent results are presented for Magnus force computations using the Cray 1S computer. Comparisons are made with the earlier CDC computer results and are further compared to some limited experimental data. A discussion of the numerical technique is included. These results represent the first computations of the Magnus effect on projectile shapes in the transonic flight regime.

II. GOVERNING EQUATIONS AND COMPUTATIONAL TECHNIQUE

The set of equations which govern fluid motion are the Navier-Stokes equations. This set of highly non-linear partial differential equations have proven extremely difficult to solve in their entirety. In most instances approximations had to be made before a solution could be attempted. For example, the well known boundary layer equations are derived by applying approximations to the Navier Stokes equations. The present solu tion technique also makes use of an approximation. The Navier-Stokes equations solved here make use of the thin-layer approximation. That is, the viscous terms are neglected in both the longitudinal and circumferential directions. The viscous terms are retained, however, in a direction nearly normal to the surface where large flow field gradients exist. This formulation retains the momentum equations in all three coordinate directions. The retention of the three momentum equations allows for the computation of separated flow and thus differs significantly from boundary layer assumptions.

The equations solved here are written in a generalized coordinate system. This allows a wide variety of body shapes to be computed using the same basic numerical technique. The notation for the physical and transformed coordinate systems are shown in Figure 1. The three dimensional, transformed, thin-layer Navier-Stokes equations, written in non-dimensional, strong conservation law form are[6]

$$\partial_\tau \hat{q} + \partial_\xi \hat{E} + \partial_\eta \hat{F} + \partial_\zeta \hat{G} = Re^{-1} \partial_\zeta \hat{S} \qquad (1)$$

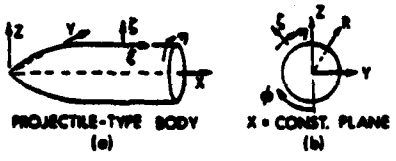

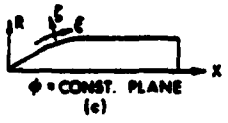

Figure 1. Physical and Transformed Coordinate System

The general coordinate transformations are defined as

$\xi = \xi(x,y,z,t)$ - longitudinal coordinate

$\eta = \eta(x,y,z,t)$ - circumferential coordinate

$\zeta = \zeta(x,y,z,t)$ - near Normal coordinate

$\tau = t$ - time

and

$$\hat{q} = J^{-1} \begin{bmatrix} \rho \\ \rho u \\ \rho v \\ \rho w \\ e \end{bmatrix} \qquad \hat{E} = J^{-1} \begin{bmatrix} \rho U \\ \rho uU + \xi_x p \\ \rho vU + \xi_y p \\ \rho wU + \xi_z p \\ (e+p)U - \xi_t p \end{bmatrix}$$

$$\hat{F} = J^{-1} \begin{bmatrix} \rho V \\ \rho uV + \eta_z p \\ \rho vV + \eta_z p \\ \rho wV + \eta_z p \\ (e+p)V - \eta_t p \end{bmatrix} \qquad \hat{G} = J^{-1} \begin{bmatrix} \rho W \\ \rho uW + \zeta_z p \\ \rho vW + \zeta_y p \\ \rho wW + \zeta_z p \\ (e+p)W - \zeta_t p \end{bmatrix}$$

The viscous matrix, $\hat{S}$, is written as

$$\hat{S} = J^{-1} \begin{bmatrix} 0 \\ \mu(\zeta_x^2+\zeta_y^2+\zeta_z^2)u_\zeta+(\mu/3)(\zeta_x u_\zeta+\zeta_y v_\zeta+\zeta_z w_\zeta)\zeta_x \\ \mu(\zeta_x^2+\zeta_y^2+\zeta_z^2)v_\zeta+(\mu/3)(\zeta_x u_\zeta+\zeta_y v_\zeta+\zeta_z w_\zeta)\zeta_y \\ \mu(\zeta_x^2+\zeta_y^2+\zeta_z^2)w_\zeta+(\mu/3)(\zeta_x u_\zeta+\zeta_y v_\zeta+\zeta_z w_\zeta)\zeta_z \\ \{(\zeta_x^2+\zeta_y^2+\zeta_z^2)[\mu/2(u^2+v^2+w^2)_\zeta+\kappa Pr^{-1}(\gamma-1)^{-1}(a^2)_\zeta] \\ +(\mu/3)(\zeta_x u+\zeta_y v+\zeta_z w)(\zeta_x u_\zeta+\zeta_y v_\zeta+\zeta_z w_\zeta)\} \end{bmatrix}$$

The velocities

$$\begin{aligned} U &= \xi_t + \xi_x u + \xi_y v + \xi_z w \\ V &= \eta_t + \eta_x u + \eta_y v + \eta_z w \\ W &= \zeta_t + \zeta_x u + \zeta_y v + \zeta_z w \end{aligned} \tag{2}$$

represent the contravarient velocities. The non-dimensional velocities U, V, and W are those components in the direction of the transformed coordinates ξ, η, and ζ, respectively. The Cartesian velocity components u, v, w together with the density ρ and total energy per unit volume e are retained as the dependent variables. The local pressure, p, is determined using the relation

$$p = (\gamma - 1)(e - .5\rho(u^2 + v^2 + w^2)).$$

The velocities are non-dimensionalized by the free stream speed of sound a_∞, the density by ρ_∞, and the total energy by $\rho_\infty a_\infty^2$. The additional parameters appearing in equation 1 are: (a) coefficient of thermal conductivity, κ; (b) dynamic viscosity, μ; (c) Reynolds number based on body diameter, Re; (d) Prandtl number, Pr, (e) λ which, based on Stokes hypothesis, is -2/3 μ.

As mentioned earlier, these equations are written in transformed coordinates; therefore, the various body shapes are introduced through determination of the metric terms ξ_x, η_x, ζ_z, etc.. These terms are formed by a combination of the derivative terms x_ζ, y_ζ, z_ζ, etc., and, together with the transformation Jacobian, allow for variable body geometries. Thus, one of the first steps in performing a computation is the generation of a computational grid which provides the x, y, z points for the metric determination. These points are determined prior to the computations and are not changed with time. Examples of the computational grid used in this study are shown in Figures 2 and 3. A two dimensional slice of the overall

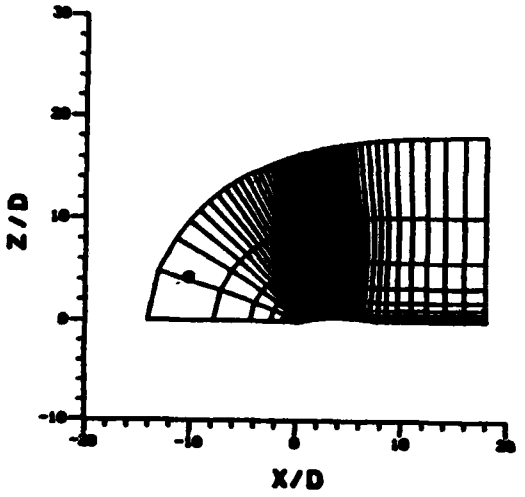

Figure 2. Physical Grid - Total Flow Field

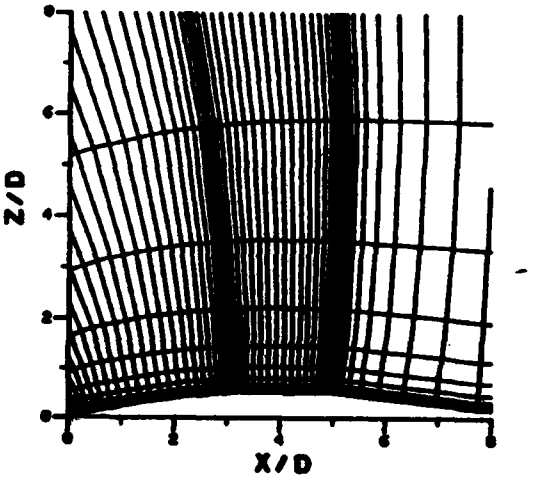

Figure 3. Physical Grid - Expanded View Near Projectile Surface

grid is shown in Figure 2. The upstream, downstream and outer flow field computational boundaries extended approximately 18 body diameters from the body surface. At this distance the flow field should be uniform and the imposed boundary conditions are considered valid. Figure 3 shows an expanded view near the body. The clustering of grid points near the body surface is required in order to resolve the viscous components of the flow field near the body surface. Due to the lack of sufficient computer storage, judicious use must be made of the limited grid points available. In regions where the viscous effects are not predominant and the flow field changes slowly, the grid points are sparse. Additional grid clustering is used in the longitudinal direction where flow field gradients are expected. The two dimensional grid shown in Figure 2 was rotated about the body axis in 10 degree increments in order to obtain the three dimensional grid required for computations at angle of attack.

As mentioned in the introduction, the Magnus effect is produced by a spin induced distortion of the boundary layer. The computation must therefore be fully three dimensional since no plane of symmetry exists. The boundary conditions used for the computations are:

(1) inner boundary, body surface

$U = W = 0$
$V = \omega$ = non-dimensional angular velocity
ρ - first order extrapolation
p - calculated using the three transformed momentum equations

(2) outer boundary

constant free stream values are used for all variables

(3) downstream boundary

$M < 1$ pressure is fixed at p_∞ and all other variables are extrapolated
$M > 1$ first order extrapolation on all variables

The numerical scheme used for the solution of equation 1 is a fully implicit, approximately factored, finite difference algorithm in delta form as analysed by Beam and Warming[7]. This scheme can be first or second order accurate in time and second or fourth order accurate in the three spatial directions. The solution of the three dimensional equations is implemented by an approximate factorization which allows the system of equations to be solved in three coupled one dimensional steps. This procedure has been utilized in previous applications[2-5] with a high degree of success. Additional details of the numerical method, computational algorithm and boundary conditions can be found in Reference 6.

The turbulence model employed is an algebraic eddy viscosity model as developed by Baldwin and Lomax[8]. This same model has yielded excellant results for Magnus effects at supersonic velocities[3].

As indicated in equation 1, this solution technique involves solving the time dependent Navier-Stokes equations. The procedure is started by assuming a uniform, free stream solution for all grid points in the computational domain. The calculation then marches in time until a steady state solution is obtained. The implicit technique used here allows for large time steps to be taken which helps to reduce the computation time.

III. MODEL GEOMETRY AND EXPERIMENT

One means of establishing the computational accuracy of a numerical scheme is through comparisons with available experimental data. The model used for the experiment and computational study presented here is an idealization of a realistic artillery projectile geometry. The experimental model shown in Figure 4 consists of a 3 caliber (1 caliber = maximum body diameter) sharp secant-ogive nose, a two caliber cylindrical mid-section, and a 1 caliber 7° conical afterbody or boattail. A similar model was used for the computational studies with the only difference being a 5% rounding of the nose tip. The nose tip rounding was done for computational efficiency and is considered to have little impact on the final integrated forces.

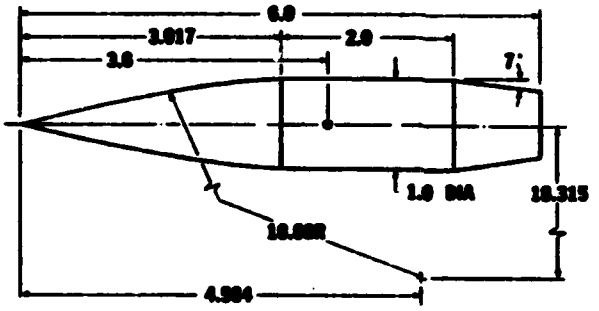

Figure 4. Model Details

The surface pressure experimental data[9] used for comparison in this paper was obtained in the NASA Langley 8 Ft. Pressure Tunnel. The test conditions of 1 atmosphere supply pressure and 320°K supply temperature resulted in a Reynolds number of 4.5×10^6 based on model length. The model was instrumented with pressure ports at 15 longitudinal stations. Pressure data and aerodynamic force data were obtained at Mach numbers of 0.91 to 1.2 and angles of attack from 0 to 10 degrees.

Additional tests were conducted at the Naval Surface Weapons Center for similar tunnel conditions. This test utilized the same model which now included the capability for spin. The model was spun to 500 rev/sec; and Magnus force and moment measurements were obtained while the model coasted down to zero spin. Aerodynamic force measurements were obtained at Mach = 0.91 for $\alpha = 0.0°$ to 10°.

IV. COMPUTER RESOURCES

The initial computations were carried out on the BRL CDC 7600 computer. This machine has a maximum large core storage capability of approximately 380,000 useable words. This limited the maximum computational grid to be 21,600 points (60 longitudinal, 20 normal and 18 circumferential). As previously mentioned the solution is marched in time until a steady state condition is obtained. A typical converged solution required approximately

1000 time steps. The CDC computation ran at a speed of 12.96×10^{-4} sec/time step/point. This resulted in 7.78 hour computation time for one converged solution at one set of conditions. As will be shown later this computational grid did not provide adequate grid resolution.

In order to obtain improved grid resolution and faster computational speed, the computer code was placed on the Cray 1S computer at Kirtland Air Force Base. Operationally, the connection to the Cray was made via the ARPANET from Aberdeen Proving Ground. The ARPANET is a Department of Defense digital switching network which allows terminals and geographically separated computers to communicate. The Cray 1S computer is a vector processor and has a demonstrated speed advantage over the CDC 7600 of 10 in the vector mode. The present computations have not yet taken full advantage of the vector capability, however. The same computation described earlier ran at a speed of 5.2×10^{-4} sec/time step/point on the Cray which resulted in a 2.5x increase in speed for the same grid. An additional advantage in using the Cray is the increased storage capability. The present configuration allows for 1 million words of storage with an expansion capability to 4 million words. The computational grid was therefore increased to 51,840 grid points (60 longitudinal, 24 normal and 36 circumferential). It was felt that increased grid resolution in the circumferential direction was required for determination of the Magnus force components. With the increased grid and same convergence criterial used earlier, the final computational time was 7.49 hours on the Cray. With full vectorization, it is anticipated that this time can be reduced to 1.5 hours. With the advent of even faster machines (Cray 2, with 32 million words of storage and speeds 6-12 times faster than the Cray 1) the eventual computational time can potentially be reduced to 15 minutes.

V. RESULTS

The results to be presented are in the form of pressure coefficients, velocity profiles and aerodynamic coefficients. The computed results are compared with the experimental data for $M = 0.91$, $\alpha = 2.0°$, and $Re = 4.5 \times 10^6$. The Magnus measurements were compared at $PD/U_\infty = 0.39$ where P = angular velocity, D = maximum body diameter and U_∞ = free stream velocity. Surface pressure comparisons are made using the Langley data, while the aerodynamic coefficient comparisons are made with the NSWC data[10].

a. Surface Pressure Coefficient

The surface pressure coefficient, $C_p = (p - p_\infty)/.5\rho_\infty U_\infty^2$, on the leeward ray is shown as a function of longitudinal position in Figure 5. The experimental data, and computational results from both the CDC 7600 and Cray 1S computers are shown. The CDC results (dashed line) show marginal

agreement with the experimental data (circles) over the entire projectile surface. The expansions and recompressions which occur near the ogive-cylinder and cylinder-boattail junction have not been adequately captured by the computation. The solid line in Figure 5 is the results from the computation on the Cray 1S computer where the grid has been expanded to 36 points circumferentially, 24 points normal to the surface and the 60 longitudinal points have been redistributed. The agreement with the experimental data has improved significantly. Some discrepancy is still apparent however, on the cylinder and on the boattail. As can be seen from Figure 3 the grid points in the vicinity of the boattail have been severely stretched and is the apparent cause of the discrepancy. All remaining results to be presented were obtained from the Cray 1S. A comparison of the windward and leeward pressure distribution is shown in Figure 6. The ogive experiences high pressure along the windward side whereas the high pressure for the boattail is on the leeward side. On the ogive, the high pressure on the windward ray causes an upward force. On the boattail, the high pressure on the leeward ray causes a negative or downward force. This condition forms a couple about the center of gravity and contributes to the critical aerodynamic behaviour which occurs at transonic velocities.

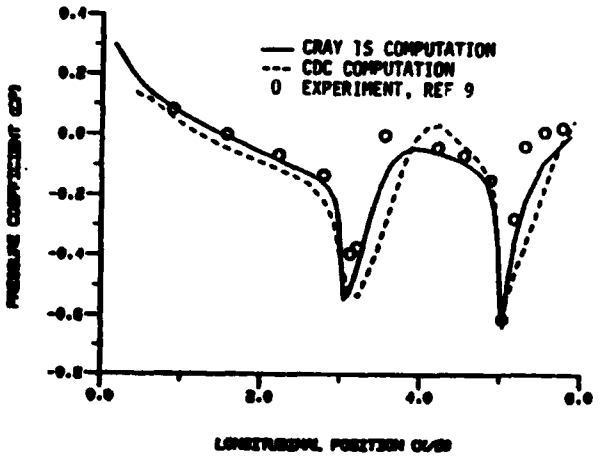

Figure 5. Surface Pressure Coefficient, Experiment and Computations, M = 0.91, α = 2.0°

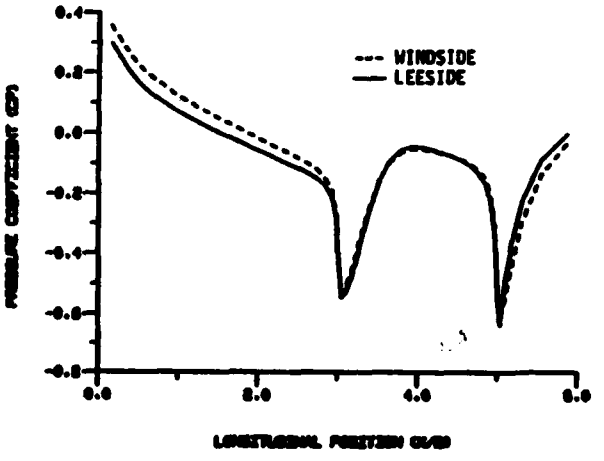

Figure 6. Windward and Leeward Surface Pressure Coefficient, M = 0.91, α = 2.0°

Comparisons between computation and experiment for the circumferential surface pressure distribution are shown in Figures 7 and 8 for X/D stations 1.56 and 5.19 respectively. As seen in these figures, the computation predicts the correct trend of the data while the actual magnitude shows a deviation. Upon close evaluation of the circumferential pressure distribution, a slight asymmetry is detected about the $\phi = 180$ plane. This condition contributes to the expected side force. The grid used for these calculations is by no means optimum and additional computational experimentation is required. The results do, however, indicate the potential for obtaining satisfactory aerodynamic coefficients. This optimism is based on results which have been obtained[5] previously for an axisymmetric computation. Figure 9 shows a comparison between experimental data and a computation using a grid consisting of 80 longitudinal points and 40 points in the near normal direction. The agreement is excellent and indicates the quality of results which should be possible for the three dimensional cases given adequate grid resolution.

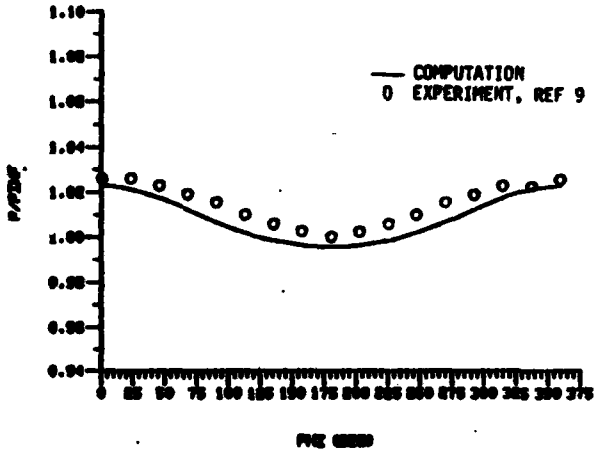

Figure 7. Circumferential Pressure Distribution, M = 0.91, α = 2.0°, X/D = 1.56

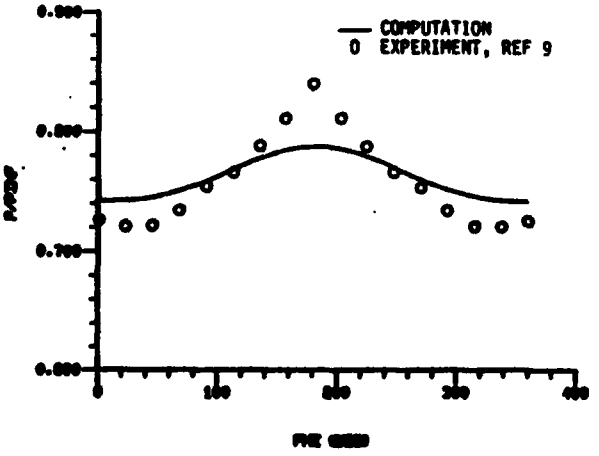

Figure 8. Circumferential Pressure Distribution, M = 0.91, α = 2.0°, X/D = 5.19

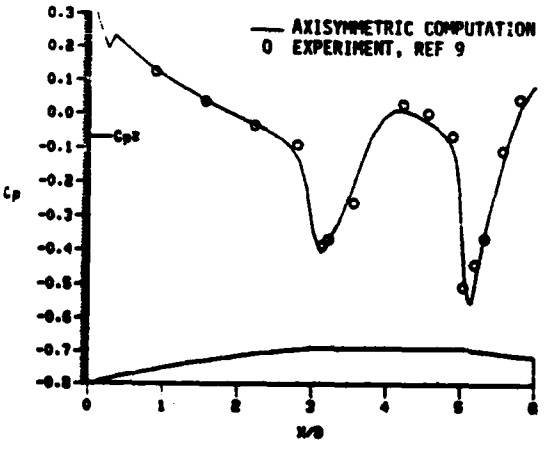

Figure 9. Surface Pressure Coefficient, Experiment and Axisymmetric Computation, M = 0.96, α = 0.0°

A primary purpose of this research effort is the development of a capability for the prediction of aerodynamic coefficients and, in particular, the capability to compute the Magnus effect. As noted, the Magnus effect is a viscous phenonena associated with the spinning projectile. Therefore, in order for a computational technique to predict this effect, it must adequately compute the longitudinal and circumferential wall shear stress for the spinning projectile at angle of attack. The experimental determination of the u, v, and w velocity distribution is especially difficult at transonic velocities. Although no experimental data are available for comparison, the computed circumferential velocity distributions are shown in Figures 10 and 11 for X/D = 4.22 and X/D = 5.50, respectively. A significant asymmetry can be seen in the velocity distributions at $\phi = 90°$ and

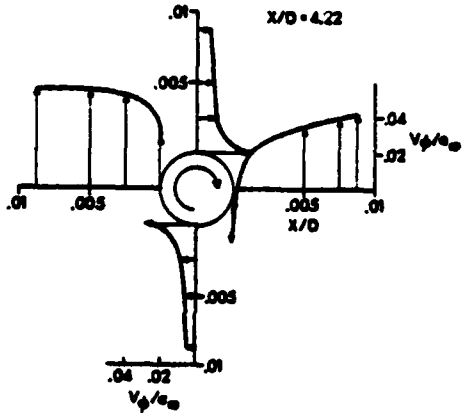

Figure 10. Circumferential Velocity Profiles for $\phi = 0°, 90°, 180°, 270°$ at M = 0.91, $\alpha = 2.0°$, X/D = 4.22

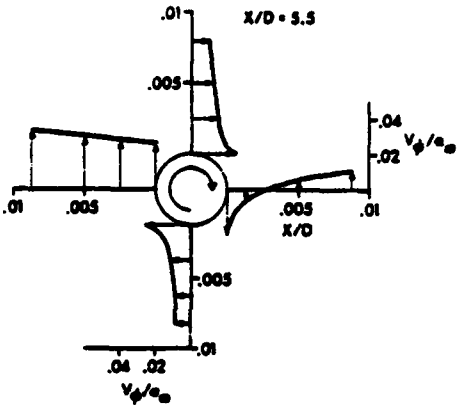

Figure 11. Circumferential Velocity Profiles for $\phi = 0°, 90°, 180°, 270°$ at M = 0.91, $\alpha = 2.0°$, X/D = 5.5

270°. At $\phi = 90°$ cross flow velocity caused by the angle of attack is in the same direction as the wall velocity. At $\phi = 270°$, the outer cross flow velocity opposes the wall velocity. The circumferential velocity of profiles at $\phi = 0°$ and $\phi = 180°$ are equally affected by the surface spin. Figure 11 shows the velocity distribution at a station midway on the boattail. The circumferential velocity distribution at $\phi = 90°$ and $\phi = 270°$ has changed significantly from that shown in Figure 10. On the boattail, the decreasing body diameter results in the surface velocity decreasing in magnitude. However, the boundary layer thickness in this region increases and the effect of surface spin is seen to persist further out.

CH PLANE AND MAGNUS COEFFICIENTS

ntegration of the pressure and viscous forces has been carried out in order to determine the aerodynamic coefficients. The sign convention used for the coefficients is shown in Figure 12. The results in Figures 13-17 are plotted as a function of longitudinal position and thus show how the force develops over the length of the projectile. Figure 13 is a plot of the normal force coefficient and shows the rapid increase in normal force which occurs on the ogive portion of the projectile. The cylinder portion

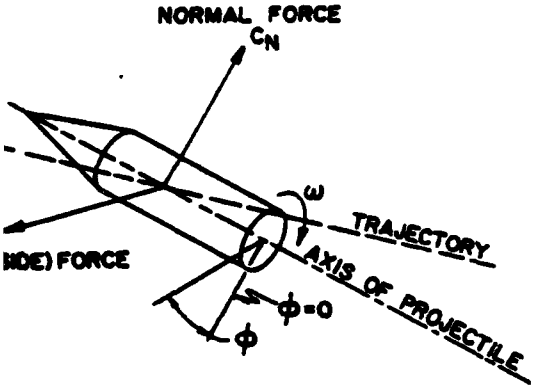

re 12. Aerodynamic Coefficient Sign Convention

roduce no significant additional normal force; however, the computndicates a slight increase in normal force here. The reversal in ction of the force on the boattail can be clearly seen as the ted normal force decreases over the length of the boattail. The ntal normal force coefficient, indicated by the circle, shows very eement with the computation.

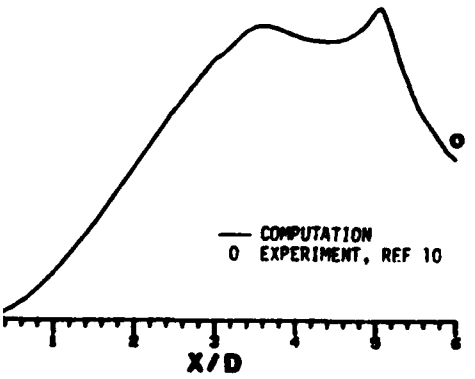

13. Normal Force Coefficient Along the Projectile, Computation and Experiment, M = 0.91, α = 2.0°

The spin rate of typical artillery shell is of the order of 300-500 rev/sec. As mentioned previously, the Magnus effect results from a spin induced distortion of the viscous boundary layer which occurs for artillery shell at angle of attack. Previous studies[1,3] have shown that the Magnus effect consists of the sum of the boundary layer displacement effect (asymmetric surface pressure distribution) plus the viscous wall shear stress contributions

$\left(\frac{du}{dy}\right)_{y=0}$ and $\tau_\phi = \mu\left(\frac{du}{dy}\right)_{y=0}$. The development of all three components agnus force are shown in Figures 14, 15, and 16 respectively, as a of longitudinal position. Both the longitudinal and circumferenponents (Figures 14 and 15) are seen to be of the order of 10^{-5} and spectively. The pressure component (Figure 16) is of the order he dominant component of the transonic Magnus effect is, therefore

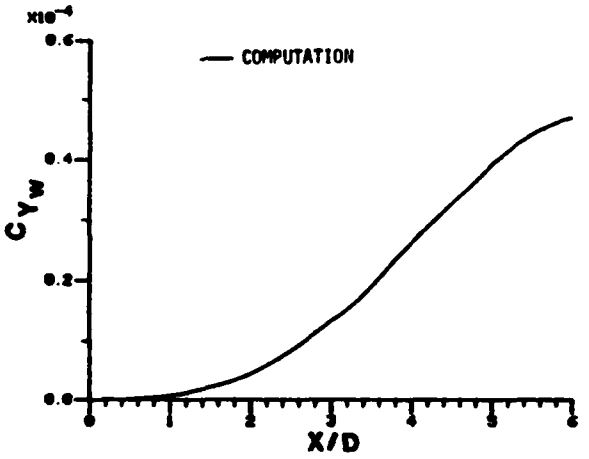

Figure 14. Circumferential Wall Shear Contribution to Magnus Force, M = 0.91, α = 2.0°, ω = 333 rev/sec

seen to be the boundary layer displacement effect, Cy_p.

Additionally, the largest portion of the total Magnus effect is seen to develop on the boattail where the viscous boundary layer reaches its maximum thickness. This is the same qualitative behavior reported by Sturek, et al[1,3] for supersonic flow. The total Magnus force ($Cy = Cy_u + Cy_w + Cy_p$) is shown in Figure 17 compared to the experimental measurement. Considering the small magnitude of the Magnus force and the agreement achieved for the normal force, the quantitative agreement between the computation and experiment is regarded as very good. The experimental Magnus force measurements were obtained in a wind tunnel not specifically designed for transonic flow and are considered to be of good qualitative value but of questionable quantitative value. Additional computations at various transonic Mach numbers and reliable experimental data are required before a full assessment of the computational technique can be made. This first result, however, for predicting the Magnus effect at transonic velocity is considered very encouraging.

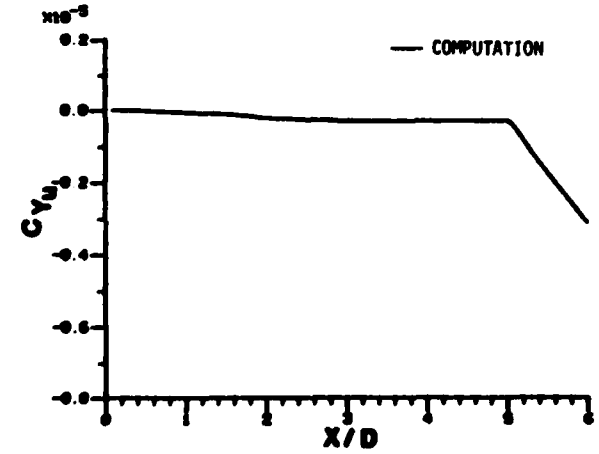

Figure 15. Longitudinal Wall Shear Contribution to the Magnus Force, M = 0.91, α = 2.0°, ω = 333 rev/sec

VII. SUMMARY

The research effort presented in this paper is part of an overall program to develop a sophisticated predictive capability for projectile aerodynamics. The pacing requirement for this capability is the determination of the Magnus force in the transonic flight regime.

An implicit finite difference code, which solves the unsteady thin-layer Navier-Stokes equations, has been applied to a projectile shape at α = 2.0°,

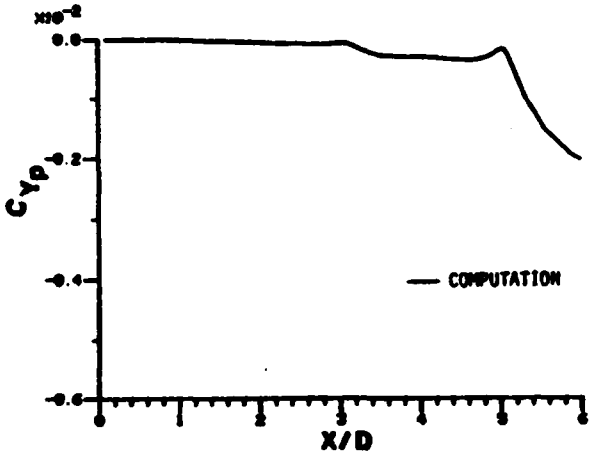

Figure 16. Circumferential Pressure Contribution to the Magnus Force, M = 0.91, α = 2.0°, ω = 333 rev/sec

tial velocity distribution, presented for significant interaction between the cross angle of attack and the body surface velocity. Experimental velocity profile data, which are very difficult to obtain for a spinning model at transonic speeds, are required to fully assess the computational results.

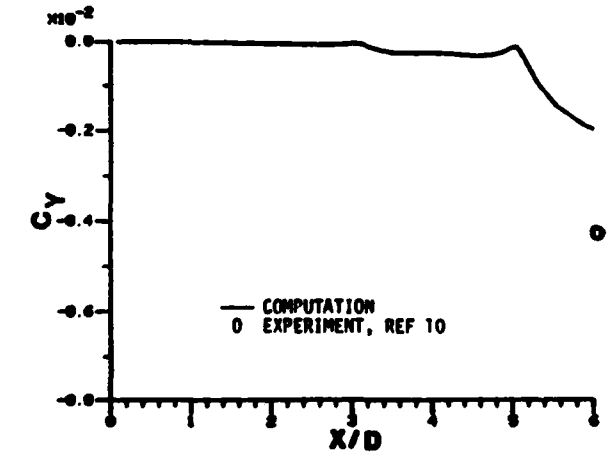

Figure 17. Total Magnus Force Along Projectile, Computation and Experiment, M = 0.91, α = 2.0°, ω = 333 rev/sec

M = 0.91. The solution was marched in time until a steady state result was obtained. Computations were first performed on a CDC 7600 using a finite difference grid of 21,600 points and required 7.78 hours of computer time. Increased grid resolution with faster computational speed per grid point was obtained by performing the computation on a Cray 1S vector computer.

The computations have been compared to experimental surface pressures and aerodynamic force coefficients. The circumferen two axial locations, showed the flow velocity resulting from The normal and Magnus force coefficients have been shown to be in good quantitative agreement with experimental data. The individual components of the Magnus force have additionally been presented and indicate qualitatively good results. The need for additional grid resolution or adaptive grid techniques[11] have been identified as a further requirement to achieve more accurate predictions. Good quality experimental, transonic Magnus data is also required for future code validation.

The present results indicate that the thin-layer Navier-Stokes computational technique, in conjunction with enhanced computer technology, has the potential of providing the capability to accurately predict the aerodynamic behavior of spinning shell at transonic velocities, including the Magnus effect.

REFERENCES

1. Sturek, W.B., et al., "Computations of Magnus Effects for a Yawed, Spinning Body of Revolution", AIAA Journal, Vol. 16, No. 7, July 1978, pp. 687-692.

2. Schiff, L.B., and Sturek, W.B., "Numerical Simulation of Steady Supersonic Flow Over Cone Ogive-Cylinder-Boattail Body", AIAA Paper No. 80-0066, January 14-16, 1980.

3. Sturek, W.B., and Schiff, L.B., "Computations of the Magnus Effect for Slender Bodies in Supersonic Flow", AIAA Paper No. 80-1586-CP, August 11-13, 1980.

4. Nietubicz, C.J., Pulliam, T.H., and Steger, J.L., "Numerical Solution of the Azimuthal-Invariant Thin-Layer Navier-Stokes Equations", AIAA Journal, Vol. 18, No. 12, December 1980, pp. 1411-1412.

5. Nietubicz, C.J., "Navier-Stokes Computations for Conventional and Hollow Projectile Shapes at Transonic Velocities", AIAA Paper No. 81-1262, AIAA 14th Fluid and Plasma Dynamics Conference, Palto Alto, CA, 1981.

6. Pulliam, T.H., and Steger, J.L., "On Implicit Finite-Difference Simulations of Three-Dimensional Flow", AIAA Journal, Vol. 18, No. 2, February 1980, pp. 159-167.

7. Beam, R., and Warming, R.F., "An Implicit Factored Scheme for the Compressible Navier-Stokes Equations", AIAA Paper No. 77-645, June 1977.

8. Baldwin, B.S., and Lomax, H., "Thin Layer Approximation and Algebraic Model for Separated Turbulent Flows", AIAA Paper No. 78-257, January 1978.

9. Kayser, L.K., and Whiton, F., "Surface Pressure Measurements on a Boattailed Projectile Shape at Transonic Speeds", to be published as a BRL Report.

10. Kayser, L.D., Ballistic Research Laboratory/ARRADCOM, Aberdeen Proving Ground, Maryland 21005, private communications.

11. Dwyer, H.A., Kee, R.J., and Sanders, B.R., "Adaptive Grid Method for Problems in Fluid Mechanics and Heat Transfer", AIAA Journal, Vol. 18, October 1980. pp. 1205-1212.